Uncertainty Quantification in Damage Modeling of Heterogeneous Materials

Michael J. Bogdanor, Sankaran Mahadevan, and Caglar Oskay*

Civil and Environmental Engineering Department, Vanderbilt University, Nashville, TN 37235, USA

Abstract

This manuscript investigates the use of Bayesian statistical methods for calibration and uncertainty quantification in rate-dependent damage modeling of composite materials. The epistemic and aleatory uncertainties inherent in the model prediction due to model parameter uncertainty, model form error, solution approximations, and measurement errors are investigated. Gaussian process surrogate models are developed to replace expensive finite element models in the analysis. A viscous damage model is employed with a solution algorithm designed for implementation within a commercial finite element software package (Abaqus). Experimental results from a suite of monotonic load tests conducted on unidirectional glass fiber reinforced epoxy composite samples at multiple strain rates and strain orientations are used to quantify the uncertainty in the prediction of the composite response within a Bayesian framework.

***Keywords**: Composite materials, Uncertainty quantification, Bayesian calibration, Rate-dependent damage, Gaussian process surrogate model.*

1. Introduction

Composite materials fail when subjected to mechanical loading in a more complicated manner than metals. Whereas metals tend to fail due to the propagation of distinct cracks, composites are susceptible to a number of interacting failure modes including fiber rupture,

* Corresponding Author: VU Station B#351831, 2301 Vanderbilt Place, Nashville, TN 37235. Email: caglar.oskay@vanderbilt.edu

matrix cracking, delamination, interface debonding, and the growth of voids within the matrix microstructure. Experiments have shown the response of composite materials to be strain-rate dependent under monotonic [1,2] and fatigue loading [3,4] for a variety of composite materials. Modeling and prediction of the response of such complex failure mechanisms requires advanced models to simulate their behavior.

Multiscale computational methods, such as the computational homogenization technique [5,6], are becoming increasingly popular for the simulation of composite materials. In these methods, the response at the scale of the microstructure is evaluated numerically over a statistically equivalent representative volume element (RVE) of the composite by considering appropriate boundary conditions and microscale constitutive relationships defined for each microconstituent within the RVE. The common approach to constitutive modeling of the composite microconstituents is employing the internal state variable theory [7], in which the stress-strain relationship at a material point within the RVE is idealized phenomenologically.

Achieving predictive capability with this approach hinges on the proper calibration of the parameters of composite microconstituents based on experimental data. Compared to calibration of single scale models, multiscale model calibration presents distinct challenges. The material parameters may be defined at disparate scales, the overall effects of which are difficult to differentiate. Model calibrations should therefore be conducted simultaneously for all or large sets of parameters. Deterministic calibration of material properties in composites has been conducted in a number of investigations using gradient-based and genetic algorithm approaches [8,9]. These calibration methods yield a single set of parameter values that are approximations of the mean parameter values, but do not capture the uncertainty in these values due to the

natural variability of the material, sparse data, errors in the model, or the possibility of multiple solutions due to the nonlinearity of the model.

In contrast to the deterministic approach, Bayesian calibration also quantifies the uncertainty in the model parameters [10,11]. The model parameter is initially defined by a prior distribution that reflects subjective knowledge (expert opinion) of its value. Typically this prior distribution represents a wide range of possible parameter values. Experimental data is then used to determine the posterior distribution of the model parameters using the likelihood of observing the experimental data for a given set of parameters. Bayesian calibration can include point data, interval data, data on statistical distributions, or any combination of these. Bayesian methods are also desirable due to their ability to quantify uncertainty from sources beyond model parameter uncertainty, including model form uncertainty, solution approximation error, and measurement error.

Markov chain Monte Carlo (MCMC) simulation is commonly used in Bayesian calibration. Several MCMC algorithms are available, such as the Metropolis-Hastings algorithm [12,13], Gibbs sampling [14], and slice sampling [15]. MCMC simulation requires several thousands of sets of samples to be evaluated using the numerical model. It quickly becomes computationally impractical to evaluate the finite element model for each set of input parameters, and therefore a surrogate model must be introduced. The surrogate model approximates the predicted response of the original model using an inexpensive function. Gaussian Process (GP) modeling is a popular choice due to its versatility in handling nonlinear relationships and the ability to estimate prediction uncertainty in the model [16,17,18]. In GP models, the prediction output is a Gaussian random field, defined by a mean and covariance function.

The objective of this paper is to quantify the uncertainty in the modeling of damage accumulation in composite materials. We propose to employ the Bayesian approach for calibration of the model parameters of composite constituents. A Gaussian process surrogate model, trained using expensive finite element model simulations, is used to efficiently approximate the solutions during the calibration process. The proposed approach is applied to evaluate the response of glass fiber reinforced epoxy composites (GFRP) subjected to a variety of loading rates.

The remainder of this manuscript is organized as follows: In Section **2**, the rate-dependent phenomenological damage evolution model for the composite material is presented. In Section **3**, issues and methods regarding uncertainty quantification of the composite material properties are discussed, including the sources of uncertainty, Gaussian process surrogate modeling, and the Bayesian calibration approach. Section **4** elaborates upon the computational implementation of the rate-dependent damage evolution using the MCMC-based Bayesian calibration method. Section **5** provides the model calibration and uncertainty quantification of glass fiber reinforced polymer composites. The parameters of the model, which govern the rate dependent behavior, are calibrated using the Bayesian approach with experimentally available results of unidirectional composite samples with different strain rates and strain orientations subjected to monotonic tensile loading.

2. Composite damage model

The composite structure is a heterogeneous body whose domain, $\boldsymbol{\Omega} \subset \mathbb{R}^d$ (where $d = 1,2,3$ denotes the spatial dimensions) as illustrated in Figure 1. The heterogeneous body is taken to be made of a periodically repeating representative volume element (RVE) with domain $\boldsymbol{\theta} \subset \mathbb{R}^d$ consisting of two or more constituent materials [19].

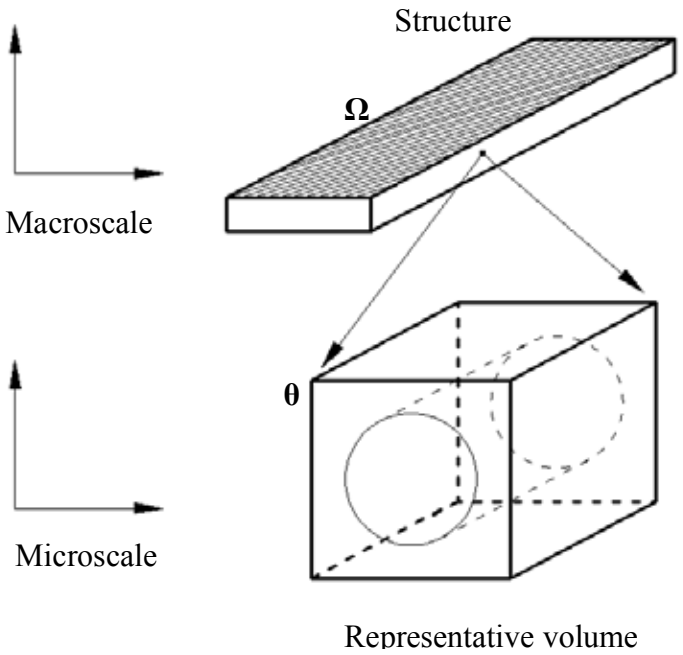

Figure 1. Multiple spatial scales.

Damage accumulation in fiber and matrix are primary failure modes for fiber reinforced composites. These failure modes have been investigated for a number of different composites [20,21,22]. Continuum damage mechanics (CDM) models utilize the internal state variable theory to idealize these failure modes, in which damage within the composite constituents is taken to follow a path-dependent evolution with respect to strain, stress or energy criterion [23]. Previous works have investigated the behavior of composites using rate-independent and rate-dependent phenomenological models [23,24,25]. In this study, a viscous damage model is used to describe the evolution of microcrack damage within the fiber and matrix phases of the composite to capture the rate-dependence observed in experiments. Damage within each microconstituent phase, $\omega_{(\alpha)}(\mathbf{x}, t)$, which varies with respect to space, $\mathbf{x}$, and time, t, within each microconstituent, reduces the stiffness of that phase such that

$$\boldsymbol{\sigma}_{(\alpha)} = \left(1 - \omega_{(\alpha)}\right)\boldsymbol{L}_{(\alpha)}\boldsymbol{\varepsilon}_{(\alpha)} \tag{1}$$

where **L** is the stiffness tensor, **σ** is the stress tensor, **ε** the strain tensor, and (α) indicates the phase of the composite (i.e. matrix, reinforcement). The evolution of damage is given by

$$\dot{\boldsymbol{\omega}}_{(\boldsymbol{\alpha})} = \dot{\boldsymbol{\lambda}} \frac{\boldsymbol{d\phi}}{\boldsymbol{dv}_{(\boldsymbol{\alpha})}} \tag{2}$$

in which the superimposed dot indicates the first derivative with respect to time, λ is the rate dependent consistency parameter, ϕ is the monotonically increasing damage hardening evolution function, $v_{(\alpha)}(\mathbf{x}, t)$ is the phase damage equivalent strain. The rate dependent consistency parameter is given as the power law expression:

$$\dot{\boldsymbol{\lambda}} = \frac{\mathbf{1}}{\boldsymbol{q}_{(\boldsymbol{\alpha})}} \langle \boldsymbol{f}\left(\boldsymbol{v}_{(\boldsymbol{\alpha})}, \boldsymbol{r}_{(\boldsymbol{\alpha})}\right) \rangle^{\boldsymbol{p}_{(\boldsymbol{\alpha})}} \tag{3}$$

where $q_{(\alpha)}$ and $p_{(\alpha)}$ are the rate dependent phase damage material parameters and f is the damage potential function, given as

$$\boldsymbol{f}\left(\boldsymbol{v}_{(\boldsymbol{\alpha})}, \boldsymbol{r}_{(\boldsymbol{\alpha})}\right) = \phi\left(\boldsymbol{v}_{(\boldsymbol{\alpha})}\right) - \phi\left(\boldsymbol{r}_{(\boldsymbol{\alpha})}\right) \tag{4}$$

If damage evolution is considered rate-independent, then $f\left(v_{ph}, r_{ph}\right) \leq 0$. This condition is relaxed for rate-dependent damage evolution and f may take on any value. Evolution of the damage hardening variable, $r_{(\alpha)}(\boldsymbol{x}, t)$, is defined as

$$\dot{\boldsymbol{r}}_{(\boldsymbol{\alpha})} = \dot{\boldsymbol{\lambda}} \tag{5}$$

and the phase damage equivalent strain is given by

$$\boldsymbol{v}_{(\boldsymbol{\alpha})} = \sqrt{\frac{\mathbf{1}}{\mathbf{2}} \left(\boldsymbol{F}_{(\boldsymbol{\alpha})}\, \hat{\boldsymbol{\varepsilon}}_{(\boldsymbol{\alpha})}\right)^{\boldsymbol{T}} \hat{\boldsymbol{L}}_{(\boldsymbol{\alpha})} \left(\boldsymbol{F}_{(\boldsymbol{\alpha})}\, \hat{\boldsymbol{\varepsilon}}_{(\boldsymbol{\alpha})}\right)} \tag{6}$$

where $\hat{\boldsymbol{\varepsilon}}_{(\alpha)}$ is the principal strain vector of the strain tensor, $\boldsymbol{\varepsilon}_{(\alpha)}$. $\hat{\boldsymbol{L}}_{(\alpha)}$ is the stiffness tensor in the principal directions, and $\boldsymbol{F}_{(\alpha)}(\boldsymbol{x}, t)$ is the weighting matrix used to account for the difference in damage accumulation between tensile and compressive loading:

$$\boldsymbol{F}_{(\alpha)} = \begin{bmatrix} \boldsymbol{h}_{1(\alpha)} & \mathbf{0} & \mathbf{0} \\ \mathbf{0} & \boldsymbol{h}_{2(\alpha)} & \mathbf{0} \\ \mathbf{0} & \mathbf{0} & \boldsymbol{h}_{3(\alpha)} \end{bmatrix} \tag{7}$$

where,

$$\mathbf{h}_{\boldsymbol{\xi}(\boldsymbol{\alpha})} = \frac{\mathbf{1}}{\mathbf{2}} + \frac{\mathbf{1}}{\boldsymbol{\pi}}\mathbf{atan}\left[\mathbf{c}_{\mathbf{1}(\boldsymbol{\alpha})}\left(\hat{\boldsymbol{\varepsilon}}_{\boldsymbol{\xi}(\boldsymbol{\alpha})} - \mathbf{c}_{\mathbf{2}(\boldsymbol{\alpha})}\right)\right] \textbf{ for } \boldsymbol{\xi} = \mathbf{1}..\boldsymbol{d} \tag{8}$$

and $c_{1(\alpha)}$ and $c_{2(\alpha)}$ are used to represent the effect of compression and tension on the evolution of damage. The damage hardening evolution function for the rate dependent model is given as

$$\phi\left(\boldsymbol{v}_{(\boldsymbol{\alpha})}\right) = \boldsymbol{a}_{(\boldsymbol{\alpha})}\left\langle \boldsymbol{v}_{(\boldsymbol{\alpha})} - \boldsymbol{v}_{\mathbf{0}_{(\boldsymbol{\alpha})}}\right\rangle^{\boldsymbol{b}_{(\boldsymbol{\alpha})}} \leq \mathbf{1} \tag{9}$$

where the $\langle\cdot\rangle$ indicates MacCauley brackets, $a_{(\alpha)}$ and $b_{(\alpha)}$ are material parameters, and $v_{0_{(\alpha)}}$ is the threshold value of strain, below which no damage accumulation occurs. The damage evolution model described by Eqs. (1)-(9) are used, along with the equilibrium equations, kinematic equations and boundary conditions, to evaluate the damage accumulation response of the composite at the scale of the representative volume.

3. Uncertainty quantification in the damage evolution model

Uncertainty in the computational simulation of natural phenomenon arises from both aleatory (irreducible) and epistemic (lack of knowledge) sources. For example, the material parameters of each composite constituent are subject to natural variability. This variability cannot be avoided, and must be quantified to inform design decisions. Epistemic uncertainty arises from

lack of adequate data, mathematical and numerical approximations used to characterize the natural behavior, and from errors in measurement of the model inputs and outputs. This uncertainty can be reduced in several ways: collect additional data, improve the accuracy of the mathematical models, employ more precise measurement techniques, or use more rigorous experimental methods. Each of these reduction measures comes at some cost. Quantification of epistemic uncertainty allows resource allocation decisions to be made to improve the model and experiments in order to reduce the overall prediction uncertainty.

The basic outline of the model used in the monotonic loading case is given in Figure 2 with the inputs, outputs, and model parameters shown with the types of uncertainty seen in each.

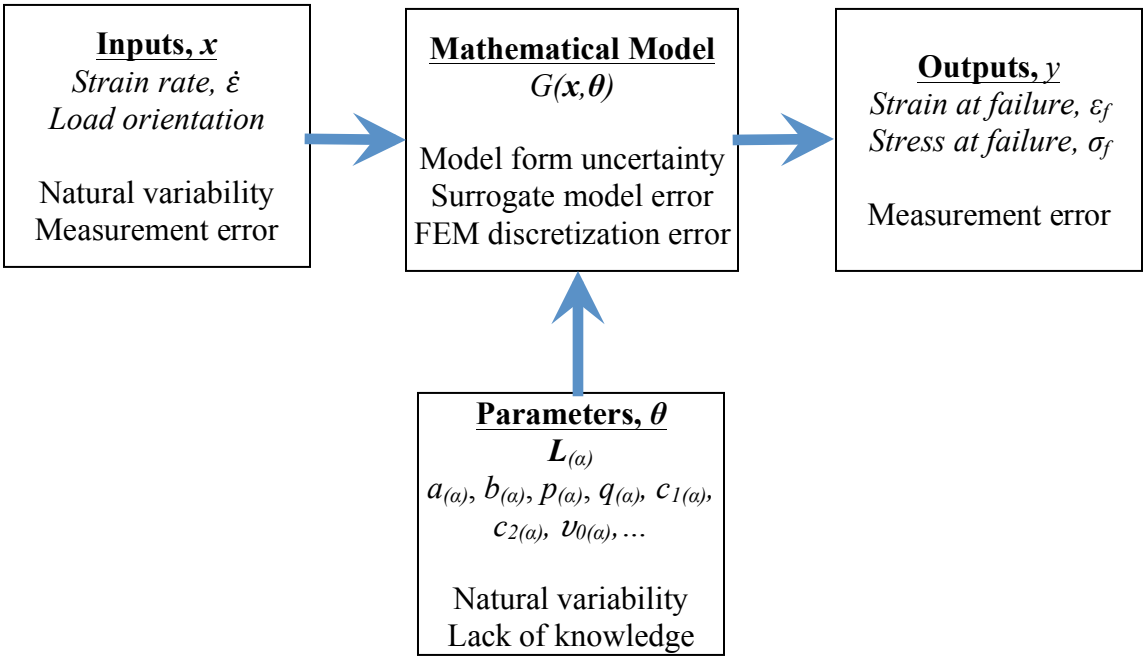

Figure 2. Uncertainty sources in model prediction.

The goal of this model is to predict the ultimate stress, σ_f, and strain, ε_f, at failure for a composite material. These are the outputs, y, of the model $G(\boldsymbol{x},\boldsymbol{\theta})$, for the inputs, $\boldsymbol{x}$, subject to the parameters, $\boldsymbol{\theta}$. The inputs for the model are the strain rate and load orientation as these are

directly controlled in the experiments. The parameters for the model are elastic properties, contained in the stiffness matrix, $\boldsymbol{L}_{(\alpha)}$, and the damage evolution parameters, $a_{(\alpha)}$, $b_{(\alpha)}$, $p_{(\alpha)}$, $q_{(\alpha)}$, $c_{1(\alpha)}$, $c_{2(\alpha)}$, and $\upsilon_{0(\alpha)}$ for each phase. In this case, the inputs are discrete values, while the model parameters are continuous. Additionally, the model $G(\boldsymbol{x},\boldsymbol{\theta})$ is a surrogate GP model that is used to approximate the output response of the finite element model, and is affected by several sources of model error.

3.1 Sources of uncertainty

The response of the composite material is subject to random natural variability. This is present in the elastic properties and the damage evolution parameters for the each phase of the composite. Epistemic uncertainty is, however, also present in these parameters from incomplete information on the distribution of the parameters. Of primary concern in this study are the parameters that govern the rate-dependency of the stress-strain response, strength and ductility modeled by the $a_{(\alpha)}$, $b_{(\alpha)}$, $p_{(\alpha)}$, and $q_{(\alpha)}$ parameters. It is difficult to analytically arrive at the distributions of these parameters directly from experimental data because the observable response of the material is non-linearly related to these parameters. What is required is an indirect calibration approach to determine the range of possible combinations of material parameters. Multiple parameters are calibrated simultaneously, thus capturing the non-linear relationships between the parameters. This is accomplished through the use of a Bayesian calibration method, discussed below.

Measurement error is present in the model inputs - strain rate and loading orientation – and outputs – macroscopic stress and strain at failure, due to imprecision in the techniques used to record these values. Slight perturbations in the experimental inputs cause the simulation model to vary from the natural behavior that is actually occurring, propagating error to the predicted

outputs. Input measurement error is assumed to be small for the experiments considered in this study and is not explicitly modeled. The uncertainty from output measurement error is commonly represented as a Gaussian random variable with zero mean and known or estimated standard deviation.

Solution approximation error exists in the model from homogenization, finite element discretization, and surrogate modeling [26]. As an example of homogenization error, the composite fiber ratio is given as an average quantity for the entire composite. However, in some areas of the material, the local fiber ratio can be significantly different from the mean. In this analysis, the stresses and strains and the fiber ratio for the composite are assumed to be uniform at the structural scale, varying only at the RVE microscale (i.e. uniform macroscopic response). The uncertainty from these homogenization assumptions could be further quantified by using RVEs of various fiber ratios, constructing macroscopic models randomly composed of these RVEs, and analyzing the resulting macrostructures for the variability in the response. There is additional model uncertainty from discretization error in the finite element model, which can be reduced by refining the mesh in the RVE. These additional finite element analyses represent significant computational expense and are not implemented in this investigation. Surrogate models that replace finite element models also contribute to approximation error. The uncertainty from the surrogate model approximation is available from the Gaussian process prediction variance and a cross-validation approach, as explained later.

A major source of epistemic uncertainty in the model comes from the model form itself. The true value of the quantity of interest, y_{true}, (e.g. σ_f or ε_f) accounting for various sources of uncertainty are:

$$\boldsymbol{y_{true}} = \widehat{\boldsymbol{y}}(\boldsymbol{x}, \boldsymbol{\theta}) + \boldsymbol{\delta}(\boldsymbol{x}) + \boldsymbol{\epsilon_m} \tag{10}$$

where $\hat{y}(\boldsymbol{x}, \boldsymbol{\theta})$ is the predicted output from the model, ϵ_m is the measurement error, and $\delta(\boldsymbol{x})$ is a model discrepancy term introduced by Kennedy and O'Hagan [27]. The $\delta(\boldsymbol{x})$ term is used to reflect discrepancy in the model prediction with respect to the experimental observations. In this paper, $\delta(\boldsymbol{x})$ includes the contributions from surrogate model error, model form uncertainty, homogenization error, and finite element discretization error. (Alternatively, one could also separately quantify the solution approximation errors and include them in Eq. 10, in order to quantify the model form error). Note that $\delta(\boldsymbol{x})$ depends on the input, $\boldsymbol{x}$. In this work, model discrepancy is a function of strain rate, where it is used to indicate rate-dependent response that is not fully characterized by the model.

3.2 Gaussian process (GP) modeling

For the MCMC method that is used in the Bayesian calibration process, several thousands of samples are required, and the computational cost of evaluating the model with finite element analysis at each of these points is prohibitively expensive. Therefore, a GP model is used as a surrogate for the full finite element analysis [17,28]. The GP model is defined such that for each input $\boldsymbol{x}$ in *D*-dimensional input space, the predicted output y_P is a Gaussian distribution. This model is "trained" with about *nt* input points, $\boldsymbol{x}_T$ using the output, y_T, using the full finite element RVE analysis for those training points where $T = 1,2..nt$. At a given prediction point, $\boldsymbol{x}_P$, the joint density of the output, conditioned upon the training point values and the parameters of the GP, is:

$$p(y_P|\boldsymbol{x}_P, \boldsymbol{x}_T, y_T; \boldsymbol{\psi}) \sim N(m, S) \tag{11}$$

where $\boldsymbol{\psi}$ are the parameters of the GP model, $\boldsymbol{m}$ is the prediction mean, and $\boldsymbol{S}$ is the prediction covariance given as:

$$\boldsymbol{m} = \boldsymbol{K_{PT}}(\boldsymbol{K_{TT}} + \boldsymbol{\sigma_n}^2\boldsymbol{I})^{-1}\boldsymbol{y_T} \tag{12}$$

$$\boldsymbol{S} = \boldsymbol{K_{PP}} - \boldsymbol{K_{PT}}(\boldsymbol{K_{TT}} + {\sigma_n}^2\boldsymbol{I})^{-1}\boldsymbol{K_{TP}} \tag{13}$$

where $\boldsymbol{K_{PT}}$ is the *np x nt* covariance matrix between *np* prediction points and the *nt* training points, $\boldsymbol{K_{TT}}$ is the *nt x nt* covariance matrix between training points, $\boldsymbol{K_{PP}}$ is the *np x np* covariance matrix between prediction points, $\boldsymbol{K_{TP}}$ is the transpose of $\boldsymbol{K_{PT}}$, and ${\sigma_n}^2$ is the noise variance in the training point. If the training points come from computational models the ${\sigma_n}^2$ term is taken to be zero. For a weakly stationary random process, i.e. covariance is only a function of the distance between two locations, the covariance, k_{ij} (elements of covariance matrices), between two points *i* and *j* is assumed to be of the squared exponential form in this paper:

$$\boldsymbol{k_{ij}} = \boldsymbol{\theta_1}\mathbf{exp}\left(-\frac{\mathbf{1}}{\mathbf{2}}\sum_{\boldsymbol{d=1}}^{\boldsymbol{D}}\frac{\left(x_{d_i}-x_{d_j}\right)^2}{{\lambda_d}^2}\right) \tag{14}$$

where θ_1 is a scaling factor on the order of output variance, ${\sigma_f}^2$, of the training output values and λ_d is a length scale parameter for each input dimension, *d*. When the process is not stationary, other covariance functions must be used (see [18]). For problems where λ_d is small, variation in the output response is more sensitive to slight perturbations of the input. When λ_d is large, the output response is not greatly affected by changes in the input. These length scale parameters are inferred in the creation of the GP model from the given data by maximizing the log marginal likelihood [17,18]:

$$\log p(y_T|\boldsymbol{x_T};\boldsymbol{\theta}) = -\frac{1}{2}{y_T}^T(\boldsymbol{K_{TT}} + \sigma_n^2\boldsymbol{I})^{-1}y_T - \frac{1}{2}\log|\boldsymbol{K_{TT}} + \sigma_n^2\boldsymbol{I}| + \frac{D}{2}\log(2\pi) \tag{15}$$

The surrogate model error is a function of the distance from a set of prediction inputs to the training points. Error is less for predictions made closer to the values used to train the response surface of the GP model, while there are high errors associated with predicting outputs for inputs

that are not near the training points. The surrogate model error can be estimated in the GP model using a jackknifing or "leave-one-out" cross-validation approach [17]. For each of the *nt* training points, a GP model is constructed leaving out the nt^{th} point. The prediction mean and variance at this point is then determined for each of the *nt* points in this manner as a Gaussian ~ *N(m,S)*. Finally, the surrogate model prediction error, ϵ_{su}, can be estimated also as a Gaussian distribution with mean, μ_{su}, and variance, σ_{su}^2, shown below:

$$\mu_{su} = \sum_{i=1}^{nt} m_i \tag{16}$$

$$\sigma_{su}^2 = \sum_{i=1}^{nt} S_i \tag{17}$$

3.3 Bayesian parameter calibration

The material parameters in the damage evolution model are calibrated here using a Bayesian approach. For the case of continuous parameter distributions, Bayes' theorem can be rewritten as:

$$f''(\boldsymbol{\theta}) = \frac{P(y_{obs}|\boldsymbol{\theta}) f'(\boldsymbol{\theta})}{P(y_{obs})} \tag{18}$$

where $\boldsymbol{\theta}$ is the set of parameters whose distributions are to be inferred from the observed data, y_{obs}. $f'(\boldsymbol{\theta})$ is the prior distribution of the parameters containing the current knowledge about the parameter, primarily from expert opinion. $f''(\boldsymbol{\theta})$ is the posterior distribution of θ given that y_{obs} has been observed, $P(y_{obs}|\boldsymbol{\theta})$ is the likelihood of observing y_{obs} for a given set of $\boldsymbol{\theta}$, and $P(y_{obs})$ is the probability that y will occur. $P(y_{obs})$ is calculated by integrating the probability of observing y over the entire space of $\boldsymbol{\theta}$. As such it is a constant in Equation 18; thus,

$$\boldsymbol{f''}(\boldsymbol{\theta}) \propto L(\boldsymbol{\theta}) f'(\boldsymbol{\theta}) \tag{19}$$

where $L(\boldsymbol{\theta})$ is the likelihood of $\boldsymbol{\theta}$ given the observed data. This likelihood function follows the form:

$$L(\boldsymbol{\theta}) = \prod_{i=1}^{nt} f_y(y_{obs(i)}|\boldsymbol{\theta}) \tag{20}$$

where $$f_y(y_i|\,\boldsymbol{\theta}) = \frac{1}{\sigma_m\sqrt{2\pi}}\, exp\,\left(-\frac{1}{2}\left(\frac{y_{P(i)}-y_{obs(i)}}{\sigma_m}\right)^2\right) \tag{21}$$

in which $y_{p(i)}$ are the predicted values of y for nt prediction points, in this case obtained from a GP model, $y_{obs(i)}$ are the observed output values, and σ_m is the standard deviation of the observation measurement error, ϵ_m, (assumed to be zero mean Gaussian).

4. Computational implementation

The response of the composite is evaluated at the scale of the microstructure using the finite element method. The user-defined material modeling capability (UMAT) was utilized in the commercial finite element modeling package, Abaqus, to implement the damage evolution law defined in Section 2. The stress update algorithm utilized to implement this model is outlined in Section 4.1. The Markov chain Monte Carlo simulation technique used to calibrate model parameters and quantify model uncertainty is shown in Section 4.2.

4.1 Stress update algorithm

The stress update algorithm that was implemented in the UMAT subroutine is defined below:

Inputs: Strain at time step k, $\boldsymbol{\varepsilon}_{(\alpha)k}$, strain increment, $\mathbf{d}\boldsymbol{\varepsilon}_{(\alpha)k}$, time step Δt, at time step k: damage, $\omega_{(\alpha)k}$, initial phase hardening value, $\mathrm{r}_{(\alpha)k}$, initial phase damage equivalent strain $\upsilon_{(\alpha)\mathrm{k}}$, and initial consistency parameter, $\dot{\lambda}_k$

Step 1: Take strain at time k+1, $\boldsymbol{\varepsilon}_{(\alpha)k+1} = \boldsymbol{\varepsilon}_{(\alpha)k} + \mathbf{d}\boldsymbol{\varepsilon}_{(\alpha)k}$

Step 2: Calculate the principal strains, $\hat{\boldsymbol{\varepsilon}}_{(\alpha)k+1}$

Step 3: Compute the weight matrix, $h_{\xi(\alpha)} = \frac{1}{2} + \frac{1}{\pi}\mathrm{atan}\,(\mathrm{c}_{1(\alpha)}(\hat{\varepsilon}_{\xi(\alpha)k+1} - \mathrm{c}_{2(\alpha)}))$

Step 4: Determine the phase damage equivalent strain, $\upsilon_{(\alpha)}$:

$$\upsilon_{(\alpha)k+1} = \sqrt{\frac{1}{2}\left(\boldsymbol{F}_{(\alpha)}\,\hat{\boldsymbol{\varepsilon}}_{(\alpha)k+1}\right)^{T}\hat{\boldsymbol{L}}_{(\alpha)}\left(\boldsymbol{F}_{(\alpha)}\,\hat{\boldsymbol{\varepsilon}}_{(\alpha)k+1}\right)}$$

Step 5: Solve for $\dot{\lambda}_{k+1}$ and $\mathrm{r}_{(\alpha)k+1}$ to satisfy

$$\dot{\lambda}_{k+1} = \frac{1}{\mathrm{q}_{(\alpha)}}\left[a_{(\alpha)}\left(\upsilon_{(\alpha)k+1} - \upsilon_{0(\alpha)}\right)^{b_{(\alpha)}} - a_{(\alpha)}\left(\mathrm{r}_{(\alpha)k+1} - \upsilon_{0(\alpha)}\right)^{b_{(\alpha)}}\right]^{\mathrm{p}_{(\alpha)}}$$

$$\text{and}\quad \mathrm{r}_{(\alpha)k+1} = \mathrm{r}_{(\alpha)k} + \left(\frac{\dot{\lambda}_k + \dot{\lambda}_{k+1}}{2}\right)\Delta t$$

Step 6: Calculate damage evolution, $\dot{\omega}$: $\dot{\omega} = \left(\frac{\dot{\lambda}_k + \dot{\lambda}_{k+1}}{2}\right) a_{(\alpha)} b_{(\alpha)} (\upsilon_{(\alpha)} - \upsilon_{0(\alpha)})^{b_{(\alpha)}-1}$

Step 7: Compute accumulated damage, ω_{k+1}: $\omega_{k+1} = \omega_k + \dot{\omega}\Delta\mathrm{t}$

Step 8: Calculate stress at time *k+1*, $\boldsymbol{\sigma}_{k+1}$: $\boldsymbol{\sigma}_{k+1} = \left(1 - \omega_{(\alpha)k+1}\right)\boldsymbol{L}_{(\alpha)} : \boldsymbol{\varepsilon}_{(\alpha)k+1}$

For each time step, Abaqus provides the initial strain, strain increment applied over the time step, length of the time step, and state variables at the start of the time step. The subroutine UMAT then calculates the strain at the end of the time step and the phase damage equivalent strain from the principal strains at the integration point. The consistency parameter, $\dot{\lambda}_{k+1}$, and phase hardening variable at the end of the time step, $r_{(\alpha)k+1}$, are solved iteratively. These values are then used to update the state variables and calculate the stress state at the integration point.

4.2 Markov chain Monte Carlo simulation with Metropolis-Hastings sampling

We consider the target distribution of the MCMC simulation as the posterior distribution $f''(\boldsymbol{\theta})$ In the Metropolis-Hastings algorithm, the following procedure is used to generate samples from the target distribution [12,17]:

Step 1: Set $i = 0$; Select a starting value $\boldsymbol{\theta_0}$ such that $f'(\boldsymbol{\theta_0}) \neq 0$

Step 2: Calculate the value of $\bar{f}(\boldsymbol{\theta}_i) = L(\boldsymbol{\theta}_i) f'(\boldsymbol{\theta}_i)$ using the observed data, $\boldsymbol{y}_{obs}$.

Step 3: Generate a random sample of inputs, $\boldsymbol{\theta}^*$, from the prior distribution

Step 4: Calculate the value of $\bar{f}(\boldsymbol{\theta}^*) = L(\boldsymbol{\theta}^*) f'(\boldsymbol{\theta}^*)$

Step 5: Calculate the acceptance ratio of the sample, $\alpha = \min\left(1, \frac{\bar{f}(\boldsymbol{\theta}^*)}{\bar{f}(\boldsymbol{\theta_i})}\right)$

Step 6: Generate a random number u, from the uniform distribution [0,1]

Step 7: If $u < \alpha$, $\boldsymbol{\theta}_{i+1} = \boldsymbol{\theta}^*$, otherwise $\boldsymbol{\theta}_{i+1} = \boldsymbol{\theta}_i$

Step 8: Increment $i = i + 1$.

Repeat 3-8 until the Markov chain converges (i.e., additional samples do not affect the distribution of the chain).

When the chain converges, the posterior distribution can be constructed using a kernel density estimation, after discarding the first few thousand burn-in samples.

5. Model calibration and uncertainty quantification in GFRP composites

The proposed model calibration and uncertainty quantification approach was employed to evaluate the response of unidirectional S2-glass/epoxy composite materials. Off-axis specimens loaded uniaxially to failure at angles of 15° and 30° to the fiber direction with strain rates of 0.0001/s, 0.01/s and 1/s, are considered. The stress strain curves for these tests provided in Ref. [2] are shown in Figure 3. The ultimate strength and the strain to failure for each of the six tests are used in the calibration effort. This data set provides a fairly sparse amount of information for calibration. As such, only a subset of the model parameters available are calibrated, specifically a_f, b_f, p_f, and q_f (f indicates the fiber phase and m the matrix).

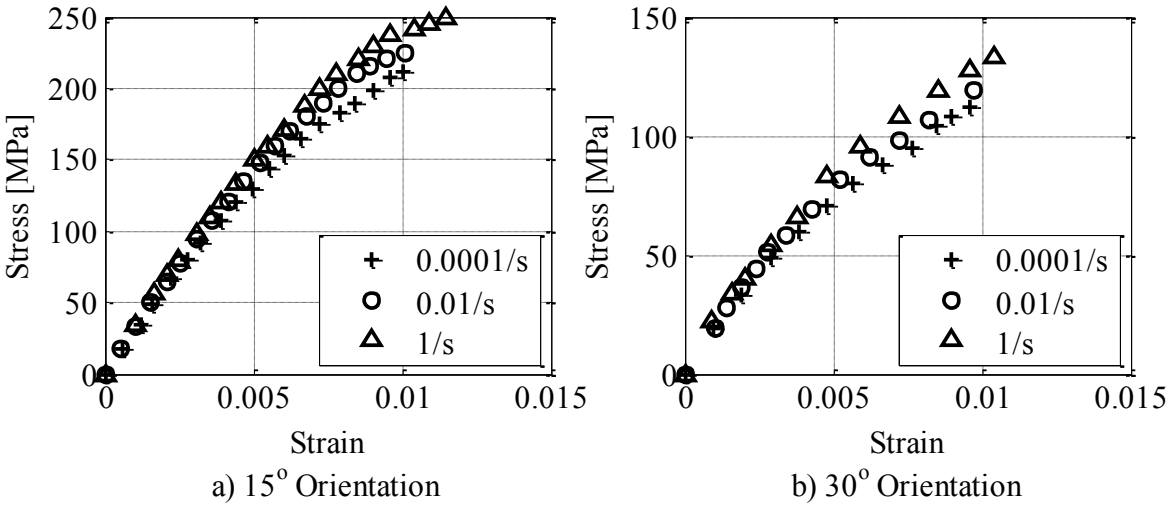

Figure 3. Uniaxial tensile stress strain curves for (a) 15° and (b) 30° off-axis specimens [2].

An RVE with a fiber ratio of 65%, shown in Figure 4, with periodic boundaries was created as a homogenization of the structural scale response for the unidirectional GFRP composite. Strain load was applied to the RVE by defining relative displacements between the periodic boundaries equivalent to the transformed strains from the off-axis loadings. The fiber and matrix phases are both made of tetrahedral elements, with 1806 total elements used to define the RVE.

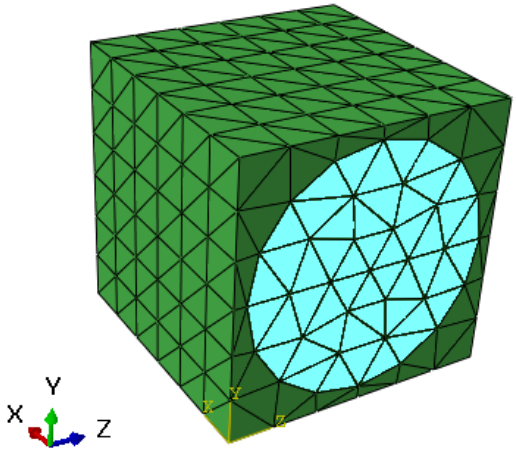

Figure 4. Representative volume element for the GFRP composite**.**

The elastic parameters of the fiber and matrix were chosen assuming isotropic behavior at the microscale such that the elastic moduli of the overall composite material at 15° and 30° to the fiber's longitudinal direction match the experimental data. The fiber is modeled with modulus of elasticity, E_f = 60 GPa, and Poisson's ratio, $\nu_f = 0.30$; the matrix with E_m = 4.775 GPa and ν_m = 0.29.

Neglecting interface damage, 14 parameters remain ($a_{(\alpha)}$, $b_{(\alpha)}$, $p_{(\alpha)}$, $q_{(\alpha)}$, $c_{1(\alpha)}$, $c_{2(\alpha)}$, and $\upsilon_{0(\alpha)}$ for both the fiber and matrix from Eq's 2,4, and 8) governing the material response of the RVE. Of these parameters, $c_{1(\alpha)}$ and $c_{2(\alpha)}$ are used to account for the difference in damage behavior under tensile and compression loadings, and are set to deterministic values, 10^5 and 0, respectively for both phases since only tension loading is considered. $\upsilon_{0(\alpha)}$, the threshold value below which no damage occurs in the phase is set to zero for both the fiber and matrix. This leaves the eight damage evolution parameters, a_m, b_m, p_m, q_m, a_f, b_f, p_f, and q_f, unknown. In this investigation, the parameters governing the matrix response are set at deterministic values (a_m = 2.0, b_m =1.5, p_m = 2.5, and q_m = 0.001) and the damage parameters of the fiber are calibrated.

The sensitivity of the damage model response to each of the four parameters, a_f, b_f, p_f, and q_f, was evaluated using a one-element model to set bounds on the prior distributions of each of these parameters in the calibration. Twelve sets of these model parameters were selected using Latin Hypercube sampling and were each used to simulate six strain rate and strain orientation input conditions from the experimental data. GP models were trained for each experiment for ultimate stress, σ_f, and strain-to-failure, ε_f. The experimental data was then used to calibrate the parameters of the damage model and discrepancy function and the standard deviation of the measurement errors. Finally, the uncertainty in the prediction is summarized and quantified.

5.1 Parameter sensitivity study

The prior distributions for the four calibrated material parameters were obtained by evaluating the damage evolution in a one-element model for the effect that each parameter displayed on the stress-strain and strain-damage relationships. The distributions of the parameters a_f, b_f, p_f, and q_f are selected, considering the nonlinear relationships in these variables, to keep the ultimate strength and strain to failure values within a reasonable range of the experimentally observed values when RVE failure occurs.

The rate of damage growth is primarily governed by a_f and b_f. As a_f increases, the strain to failure decreases and the maximum stress attained decreases, seen in Figure 5. Figure 6 shows the effects of b_f on stress, strain, and damage with damage accumulating faster for larger b_f values, accompanied by lower stress values.

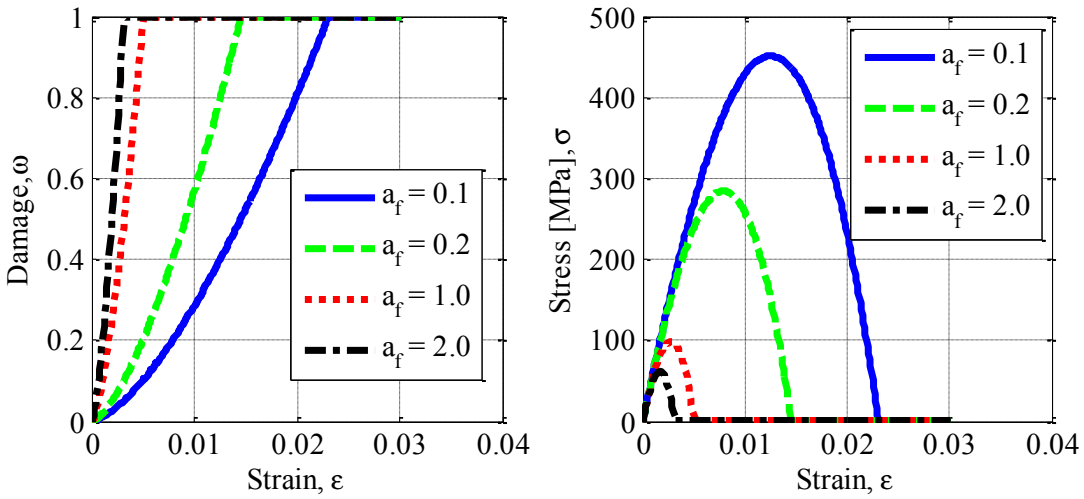

Figure 5. Effect of a_f on damage-strain and stress-strain.

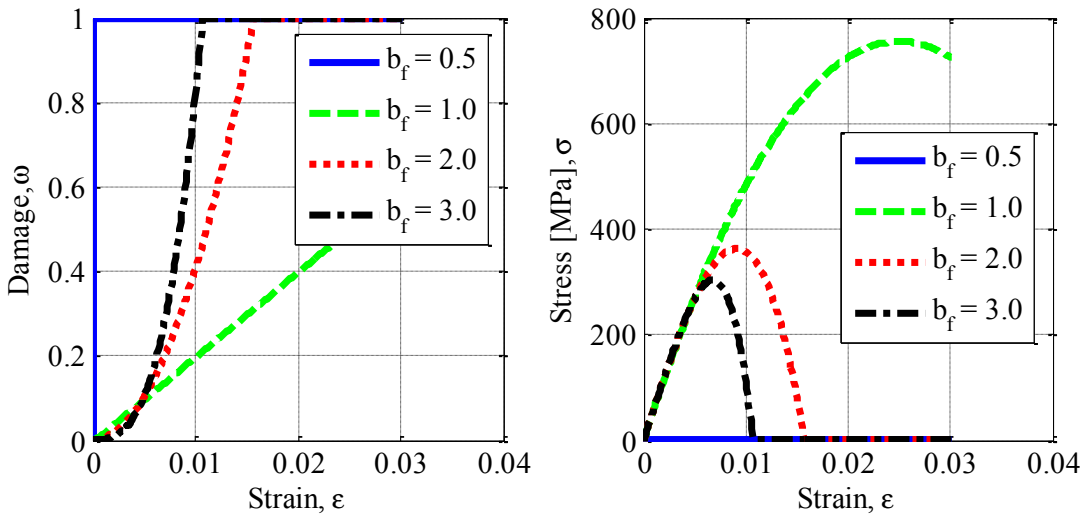

Figure 6. Effect of b_f on damage-strain and stress-strain.

The parameters p_f and q_f govern the rate-dependency of the damage evolution. Figure 7 shows the effect of three different values of p_f for each of the strain rates considered. As p_f increases, the response becomes more rate-dependent. Figure 8 shows the effect of q_f on the rate dependency of the damage accumulation model. For greater q_f values, the difference between growth rates from different strain rates is more pronounced.

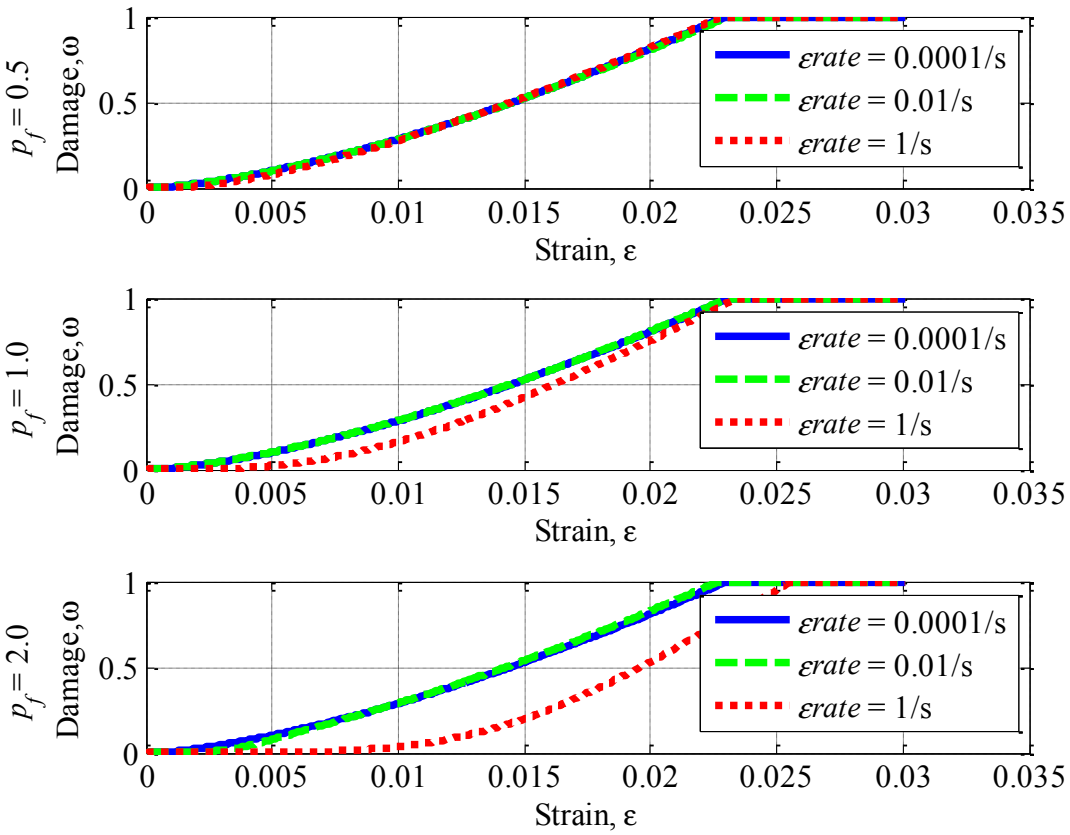

Figure 7. Effect of p_f and strain rate on damage accumulation.

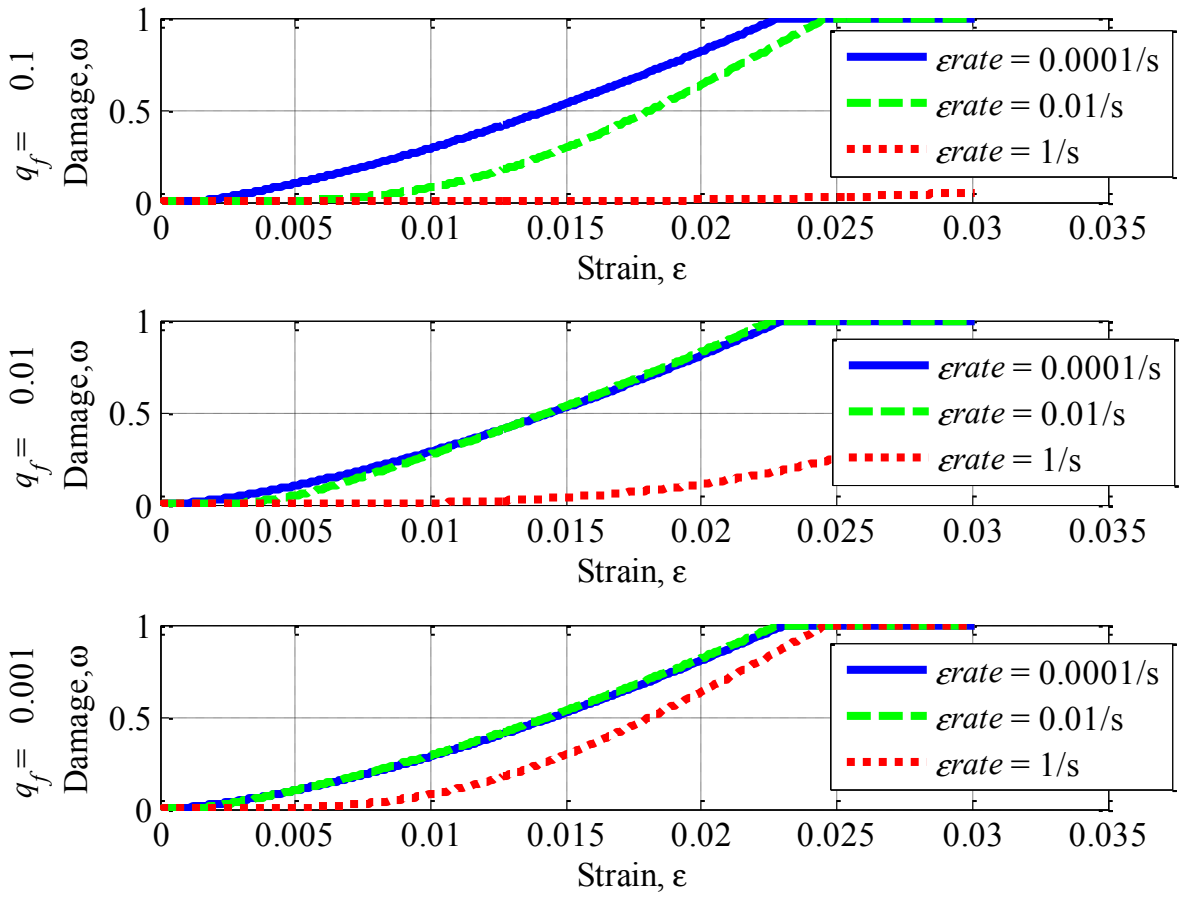

Figure 8. Effect of q_f and strain rate on damage accumulation.

This analysis yields prior uniform distributions for the parameters as $a_f = [0,0.2]$, $b_f = [1,2]$, $p_f = [1,2]$, and $q_f = [0,0.001]$.

5.2 Simulation and GP model training

Using Latin Hypercube sampling to draw twelve sets of model parameter values from the prior distributions above and the six experimental input conditions, 72 finite element simulations were performed. From these simulations, the stress at the macroscale of the composite was calculated as the component of the homogenized stress acting in the direction of the strain loading. As the RVE was loaded with the strain oriented at an angle to the fiber direction, the

face of the RVE transverse to the fiber direction accumulates damage at the fastest rate (see Figure 9). Structural failure occurs when the stress carrying capacity in this direction is lost. The resulting stress-strain curves from all 72 simulations are shown alongside the experimentally obtained curves in Figure 10.

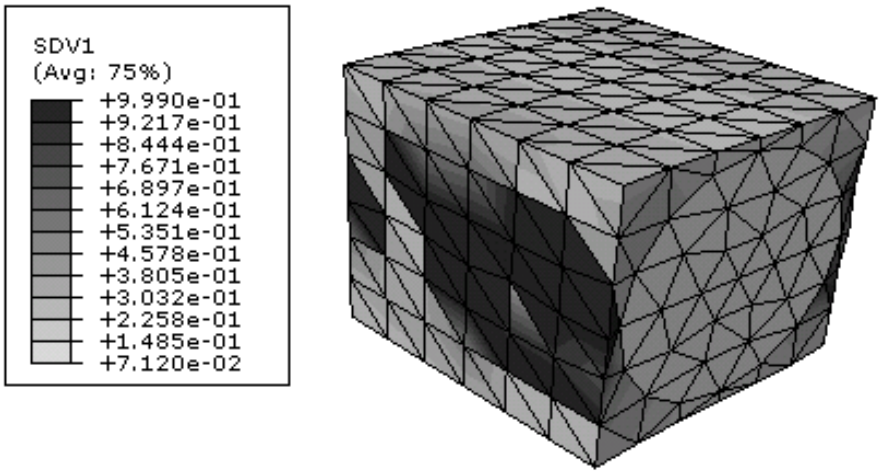

Figure 9. Damage accumulation transverse to the fiber direction.

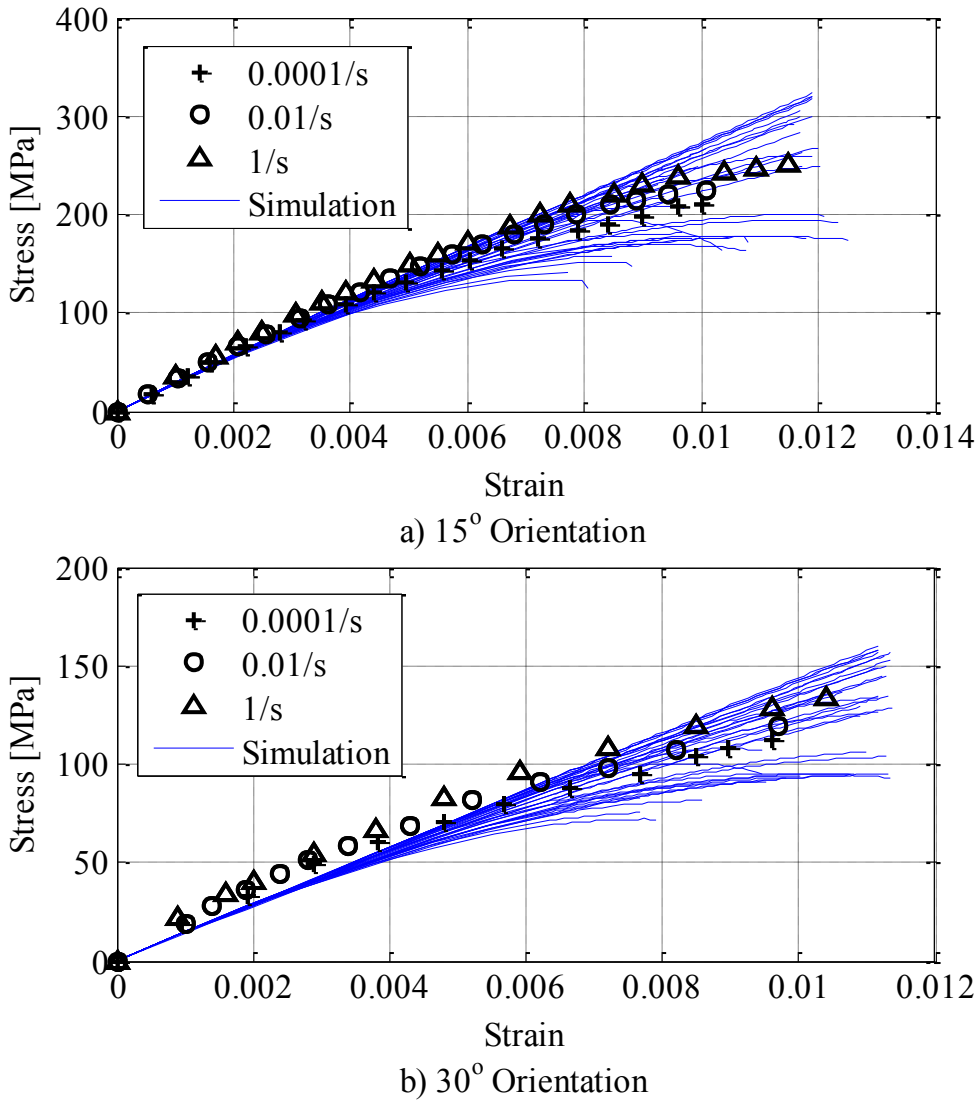

Figure 10. Simulated vs. Experimental stress-strain curves for (a) 15° and (b) 30° strains.

The ultimate stress and the strain-to-failure from these simulations were then used to train twelve GP models. A mean (trend) function was used in the training of the GP models as a first fit for the outputs to the model parameters. To account for the nonlinearity in the model, the form of the mean function was:

$$\hat{y}_{mean} = c_0 + c_1 a_f + c_2 b_f + c_3 {a_f}^2 + c_4 {b_f}^2 + c_5 {a_f}^3 + \frac{c_6}{a_f b_f} + c_7 p_f + c_8 \ln(q_f) \qquad \textbf{(22)}$$

where $\hat{y}_{mean}$ is the mean function prediction and $c_{0..8}$ are the coefficients of the mean function. These coefficients were determined from least-squares regression for each of the twelve surrogate models and the GP model with a squared exponential covariance function was then trained using the difference between the mean function prediction and the actual training value. Using this form for the mean function yielded predictions with R-squared values from 0.9 to 0.99 for each of the twelve data sets.

5.3 Model discrepancy and measurement error

Recalling Eq. (10), the GP model provides the prediction, $\hat{y}(\boldsymbol{x}, \boldsymbol{\theta})$, while the discrepancy, $\delta(\boldsymbol{x})$, and measurement error, ϵ_m, must still be addressed. In this study, it was assumed that the model discrepancy is only a function of the strain-rate, $\dot{\varepsilon}$, and that the function is the same for both the 15° and 30° tests:

$$\delta(\boldsymbol{x}) = b_0 + b_1 ln(\dot{\varepsilon}) \tag{23}$$

where b_0 and b_1 are the coefficients of the discrepancy term to be calibrated (two for the stress discrepancy and two for the strain discrepancy). The prior distributions for these coefficients are taken as uniform: $b_{0\_\sigma} = [-10,10]$, $b_{1\_\sigma} = [-2,2]$, $b_{0\_\varepsilon} = [-1,1]$, $b_{1\_\varepsilon} = [-0.01,0.01]$.

Output measurement error is taken as a Gaussian random value with zero mean and standard deviation, σ_m. Since two types of outputs, ultimate stress and strain-to-failure are utilized in this calibration process, two separate values of measurement error standard deviation are calibrated, σ_{m_σ} and σ_{m_ε}, for the stress and strain respectively. The prior density of the standard deviation, based on the Fisher information criterion [29] is given as:

$$f'(\sigma) \propto \frac{1}{\sigma} \tag{24}$$

In the calibration, the prior of the standard deviation was assumed to be uniform from 0 to 20 MPa for stress and 0 to 0.1% for strain.

5.4 Calibration results

The distributions of ten variables are to be calibrated using MCMC sampling: $\boldsymbol{\theta} = \{a_f, b_f, p_f, q_f, b_{0\_\sigma}, b_{1\_\sigma}, b_{0\_\varepsilon}, b_{1\_\varepsilon}, \sigma_{m\_\sigma}, \sigma_{m\_\varepsilon}\}$. For each loop in the MCMC sampling, a random value was sampled from each distribution. Assuming independence, the prior probability of this set is then proportional to the product of the inverse of the standard deviations, as all the other values are sampled from uniform distributions. Using a_f, b_f, p_f, and q_f, the GP model predictions for the twelve outputs were calculated. The discrepancy values were calculated from b_{0_σ}, b_{1_σ}, b_{0_ε}, and b_{1_ε} using Eq. 23, and added to the GP prediction. The measurement error standard deviations σ_{m_σ}, and σ_{m_ε} were then used to calculate the likelihood of observing the experimental outputs given those model parameters and discrepancy values. MCMC simulation was then carried out for five hundred thousand samples until the chain converged.

The results for the calibrated distributions of the four model parameters are shown in Figure 11 through Figure 14. In each of the graphs, posterior distribution of the parameters can be seen to tighten and show preference to a narrower band of values. Each of the graphs shows one major spike in the parameter values, with some minor spikes away from the large spike. This is partly attributed to the nonlinearity of the model and numerical artifacts from the MCMCS method.

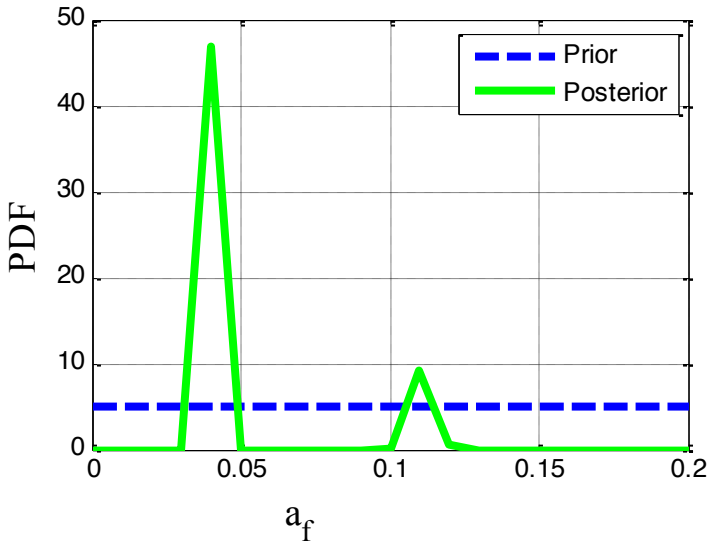

Figure 11. Calibrated distribution of a_f.

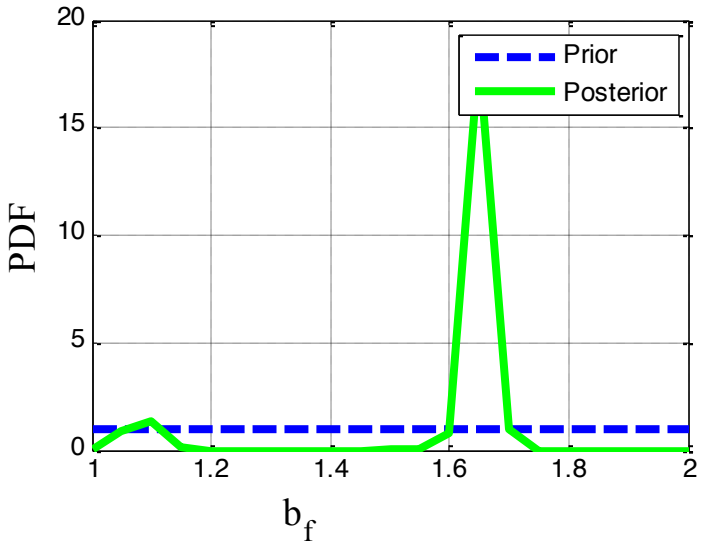

Figure 12. Calibrated distribution of b_f.

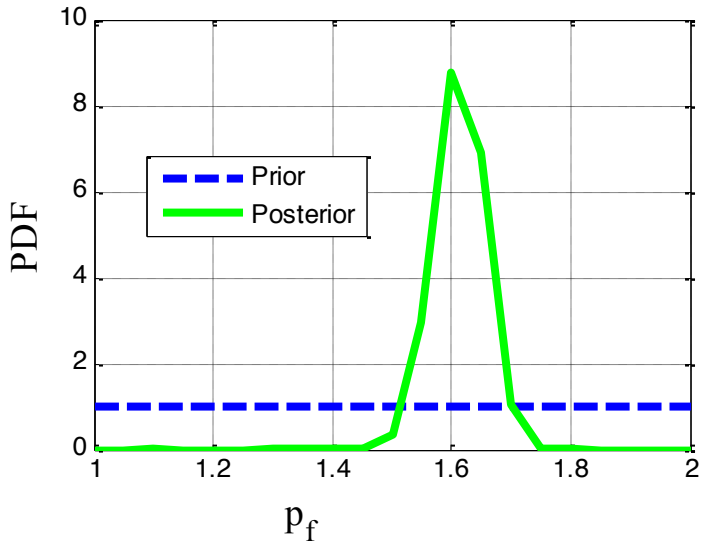

Figure 13. Calibrated distribution of p_f.

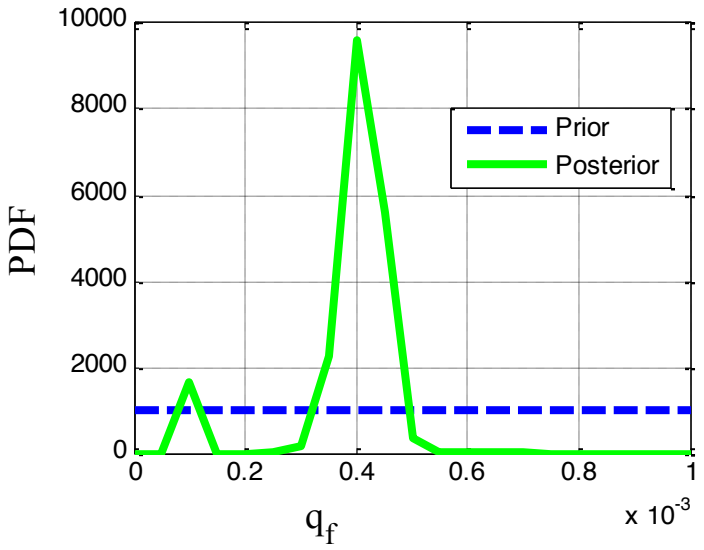

Figure 14. Calibrated distribution of q_f.

5.5 Prediction uncertainty quantification

Apart from the natural variability in the material parameters, two major sources of uncertainty exist in the model: model discrepancy and measurement error. Surrogate model error was estimated by using the "leave-one-out" approach. In the calibration procedure, this

surrogate model error is included in the calibrated model discrepancy. Model discrepancy and measurement error were evaluated during the calibration process.

The estimated error in the surrogate model is given in Table 1. The variance in the stress prediction error was high indicating that additional training points are needed to reduce the epistemic uncertainty. With four parameter dimensions, twelve training points can miss nonlinearities in the model response.

Table 1. GP surrogate model error.

			Surrogate Model Error	
Output	**Strain Rate**	**Strain Orientation**	**Mean**	**Variance**
Stress	0.0001/s	15°	0.0142	53.1
Stress	0.01/s	15°	-0.0050	37.5
Stress	1/s	15°	-0.5016	134.4
Stress	0.0001/s	30°	-0.0777	5.6
Stress	0.01/s	30°	-0.0616	1.4
Stress	1/s	30°	-0.2251	30.9
Strain	0.0001/s	15°	0.001172	0.000479
Strain	0.01/s	15°	0.000690	0.000186
Strain	1/s	15°	-0.000487	0.001545
Strain	0.0001/s	30°	-0.000197	0.000315
Strain	0.01/s	30°	0.000270	0.000487
Strain	1/s	30°	-0.000075	0.001293

The parameters of the model discrepancy (including model form error and solution approximation error) calibrated simultaneously with the model parameters are shown in Figure 15 for stress and Figure 16 for strain. If there were no discrepancy in the model, each of the coefficients would be equal to zero. As this is not the case, it is apparent that the damage model or surrogate model has discrepancy in capturing all of rate-dependent effects in the material response.

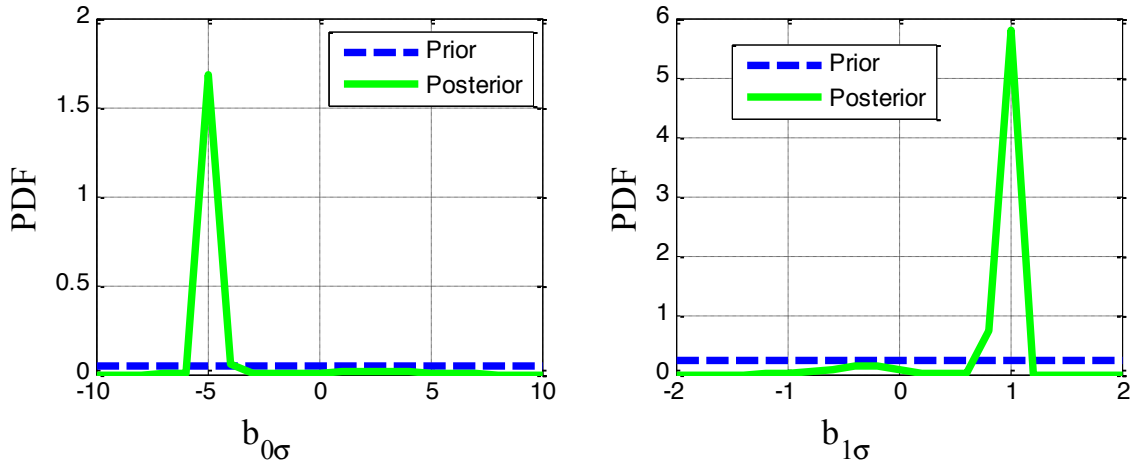

Figure 15. Model discrepancy parameters for stress ($\delta(\boldsymbol{x}) = b_0 + b_1 \ln(\dot{\boldsymbol{\varepsilon}})$).

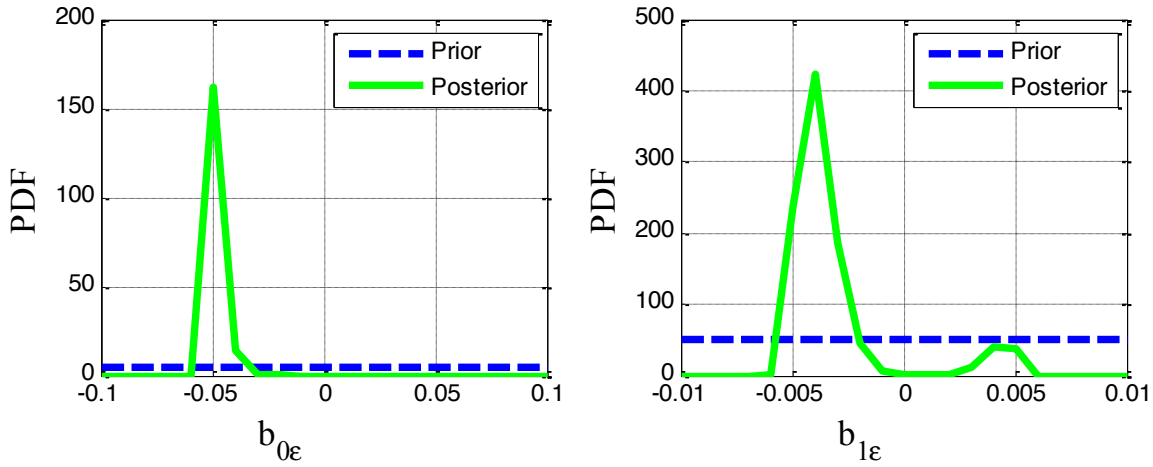

Figure 16. Model discrepancy parameters for strain ($\delta(\boldsymbol{x}) = b_0 + b_1 \ln(\dot{\boldsymbol{\varepsilon}})$).

The final uncertainty measure that was calibrated is the standard deviation of the measurement error. The posterior distributions for stress and strain measurements are displayed in Figure 17. These graphs indicate that the standard deviation of the measurement error in the stress is around 2 MPa and for strain around 0.01%.

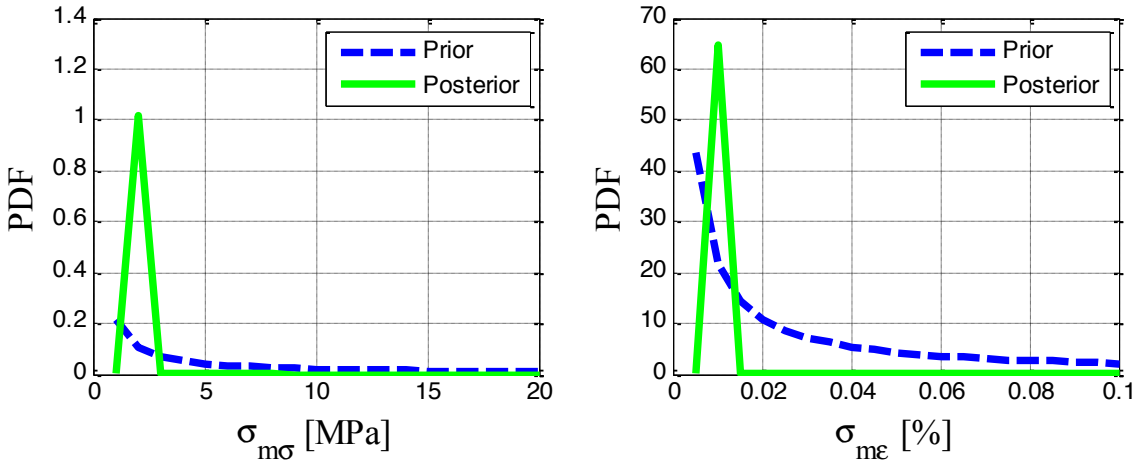

Figure 17. Measurement error standard deviation.

The calibrated model parameters were used to draw samples of the predicted outputs using Eq. (10). This prediction for the first experimental set-up with a 0.0001/s strain rate and strain applied at a 15° angle to the fiber direction is shown in Figure 18. A significant amount of scatter remains around the observed value for the output, but the calibration shows reasonable performance in achieving results close to the observations. While the range of predicted strain to failure appears to be centered on the observed results, the range of predicted ultimate stress tends to be biased below the observed value. The calibration and prediction accuracy can be improved with further testing and a larger data set.

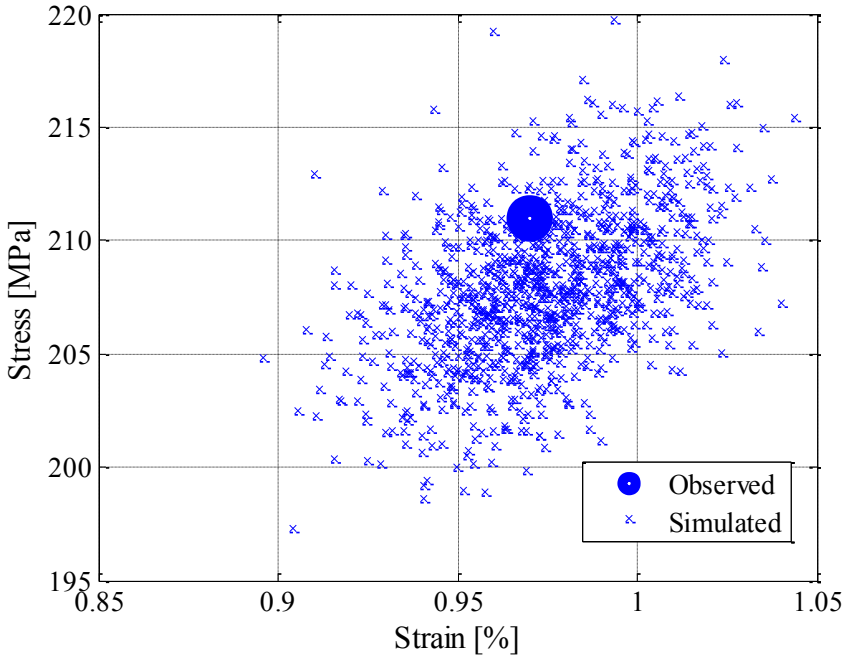

Figure 18. Predicted Outputs for 0.0001/s at 15°.

6. Conclusion

In this study, a Bayesian approach was used to calibrate the model parameters in the rate-dependent composite material damage evolution model from experimental data. This calibration yielded distributions for the material parameters of the damage evolution model for the composite constituents and the standard deviation of the measurement errors, σ_{m_σ}, and σ_{m_ε}. Gaussian process models were implemented in this task as surrogate models for expensive finite element analyses, and the approximation errors from these surrogate models was quantified.

Nonlinear behavior, lack of extensive test data, and incomplete understanding of the material phenomenology contribute to errors in the prediction of composite material response. Rate dependency in the damage model was controlled by the parameters $p_{(\alpha)}$, and $q_{(\alpha)}$, but these might not fully capture this effect, as evinced by the large discrepancy values.

Ultimately, further experimental testing is needed to improve the accuracy of the calibration and better quantify the measurement errors. Additional GP model training points are needed to more fully characterize the response surface across the entire parameter input space and reduce the uncertainty contribution from the surrogate model.

Propagation of uncertainty across multiple spatial and time scales as seen in fatigue loading is of important concern for economic design of composite materials. The next step in this research is to extend the viscous damage evolution to multi-scale applications, considering the cyclic fatigue loading.

References

1 J. Raghavan and M. Meshii. Time-dependent damage in carbon fibre-reinforced polymer composites. *Composites Part A: Applied Science and Manufacturing*. 27(12):1223-1227, 1996.

2 S.V. Thiruppukuzhi, C.T. Sun. Models for the strain-rate-dependent behavior of polymer composites. *Composite Science and Technology*. 61(1):1-12, Jan 2001.

3 J. Aronhime, H. Harel, A. Gilbert, and G Marom. The Rate-dependence of Flexural Shear Fatigue and Uniaxial Compression of Carbon- and Aramid-fibre Composites and Hybrids. *Composite Science and Technology* 43(2):105-116, 1992.

4 H.S. Chen, S.F. Hwang, and H.S. Chen. Accelerated Fatigue Properties of Unidirectional Carbon/Epoxy Composite Materials. *Polymer Composites*. 138-146. 2006.

5 J.M. Guedes and N. Kikucki. Preprocessing and postprocessing for materials based on the homogenization method with adaptive finite element models. *Computational Methods in Applied Mechanics and Engineering*, 83:143-198, 1990.

6 K. Terada and N. Kikuchi. Nonlinear homogenization method for practical applications. In S. Ghosh and M. Ostoja-Starzewski, editors, *Computational Methods in Micromechanics*, AMD-212/MD-62:1-16. ASME, 1995.

7 J. Lemaitre, J.L Chaboche. Mechanics of Solid Materials. Cambridge University Press. 1994.

8 C. Oskay and J. Fish. On Calibration and Validation of Eigendeformation-based Multiscale Models for Failure Analysis of Heterogeneous Systems. *Computational Mech*anics 42:181-195. 2008.

9 T.R. Emery, J.M. Dulieu-Barton, J.S. Earl, P.R. Cunningham. A generalized approach to the calibration of orthotropic materials for thermoelastic stress analysis. *Composite Science and Technology* 68(3-4):743-752, Mar. 2008.

10 P.M. Reilly and H. Patino-Leal. A Bayesian study of the error-in-variables model. *Technometrics*, 221-231, 1981.

11 R. Zhang and S. Mahadevan. Model Uncertainty and Bayesian Updating in Reliability-Based Inspection. *Structural Safety*. 22:145-160, 2000.

12 N. Metropolis, A.W. Rosenbluth, M.N. Rosenbluth, A.H. Teller, and E. Teller. Equation of state calculations by fast computing machines. *The Journal of Chemical Physics*, 21(6):1087, 1953.

13 W.K. Hastings. Monte Carlo sampling methods using Markov chains and their applications. *Biometrika*, 57(1):97, 1970.

14 D. Geman, S. Geman. Stochastic relaxation, Gibbs distributions, and the Bayesian restoration of images. *IEEE Transactions on Pattern Analysis and Machine Intelligence*, 14:721-741. 1984.

15 R.M. Neal. Slice Sampling. *Annals of Statistics*, 705-741, 2003.

16 S. Sankararaman. Uncertainty Quantification and Integration in Engineering Systems. PhD Thesis, Doctoral Thesis Dissertation. Vanderbilt University, Nashville, TN, 2012.
17 V. Hombal, S. Mahadevan, Bias Minimization in Gaussian Process Surrogate Modeling for Uncertainty Quantification. *International Journal for Uncertainty Quantification* 1 (4): 321-349. 2011.
18 C. Rasmussen, C. Williams. *Gaussian Processes for Machine Learning.* Springer, New York, 2006.
19 R. Crouch and C. Oskay. Symmetric Meso-Mechanical Model for Failure Analysis of Heterogeneous Materials. *International Journal Multiscale Computational Engineering*, 8:447-461, 2010
20 X. Huang, J.W. Gillespie, R.F. Eduljee, Z. Shen. Matrix Cracking Behavior of K3B/IM7 Composite Laminates subject to Static and Fatigue Loading. *Composite Structures* 49(4):435-441, Aug 2000.
21 T.P. Philippidis and T.T. Assimakopoulou. Strength Degredation due to Fatigue-induced Matrix Cracking in FRP Composites: An Acoustic Emission Predictive Model. *Composite Science and Technology* 68(15-16):3272-3277, Dec 2008.
22 C. Oskay and J. Fish. On Calibration and Validation of Eigendeformation-based Multiscale Models for Failure Analysis of Heterogeneous Systems. *Computuational Mech*anics 42:181-195. 2008.
23 J.C. Simo, J.W. Ju. Strain- and Stress-based Continuum Damage Models – II. Computational Aspects. *International Journal of Solids and Structures*, 23(7):841-869, 1987.
24 R. K. Abu Al-Rub, G. Z. Voyiadjis. A Finite Strain Plastic-damage Model for High Velocity Impact using Combined Viscosity and Gradient Localization Limiters: Part I – Theoretical Formulation. *International Journal of Damage Mechanics*, 15:293-334, 2006.
25 J. Aboudi. The Effect of Evolving Damage on the Finite Strain Response of Inelastic and Viscoelastic Composites. *Materials*, 2:1858-1894, 2009.
26 B. Liang, S. Mahadevan, Error and Uncertainty Quantification and Sensitivity Analysis of Mechanics Computational Models. *International Journal for Uncertainty Quantification.* 1(2):147-161. 2011.
27 M.C.Kennedy, A. O'Hagan. Bayesian calibration of computer models. *Journal of the Royal Statistical Society: Series B (Statistical Methodology)*. 63(3):425-464. 2001.
28 S. Sankararaman, Y. Ling, S. Mahadevan. Model Validation and Uncertainty Quantification of Fatigue Crack Growth Analysis. *Engineering Fracture Mechanics*. 78(7):1487-1504. 2011.
29 H. Jeffrys. An Invariant form for the prior probability in estimation problems. *Proceedings of the Royal Society of London. Series A, Mathematical and Physical Sciences*, pages 453-461. 1946.